Many-electron redistribution in *n*-doped semiconductor nanostructures under external electric field by using a center-of-mass approach

Reyna Méndez-Camacho,[1,2,*] Ramón Castañeda-Priego,[1] and Esteban Cruz-Hernández[2,†]
[1]*División de Ciencias e Ingenierías, Campus León, Universidad de Guanajuato, Loma del Bosque 103, 37150 León, México*
[2]*Coordinación para la Innovación y Aplicación de la Ciencia y la Tecnología, Universidad Autónoma de San Luis Potosí, Sierra Leona 550, 78210 San Luis Potosí, México*

(Received 19 April 2020; revised 13 June 2020; accepted 16 June 2020; published 1 July 2020)

The study of an external force triggering the many-electron redistribution in nanostructures is of importance for both theoretical and practical interest in condensed matter physics. Hence, the goal of this contribution is to theoretically investigate the influence of an external electric field (EEF) on the ground and excited states of a system of many-electrons confined in GaAs/AlGaAs nanostructures. To deal with the many-body issue, we employ a Yukawa-like potential in a two-electron framework, while it is proposed to explore the challenging EEF contribution by analyzing its effect on the electronic center-of-mass framework. Thus, while the Yukawa-like potential allows us to model the many-electron interaction in the range from 10^{17} to 10^{23} electrons/cm^3, via the adjustment of a simple screening parameter; the center-of-mass approximation also allows us to describe easily the effect of the EEF separately. Internal electronic distributions in nanostructures of various sizes and electronic concentrations are obtained and discussed for EEF of variable magnitude. This alternative approach enables us to decouple the electron-electron and the EEF interactions, which is useful in determining the origin of the observed features. We show that this theoretical framework is well suited to get relevant information in semiconductor nanostructures of practical sizes and realistic doped levels.

DOI: 10.1103/PhysRevB.102.035403

I. INTRODUCTION

Recent advances in nanofabrication and the technology of semiconductor nanostructures, such as quantum wires (QWRs) or quantum dots (QDs) [1–3], promise a wide spectrum of potential applications. The latter are possible due to the deep modification of the nanostructure physical properties, such as sharp density of states, ballistic electronic transport, or enriched optical properties that are quite different to those of the bulk material [3,4].

In particular, because QWRs possess both transversal quantum confinement and longitudinal ballistic transport, extensive experimental and theoretical studies [5–8] have shown their high potential to be applied in the next generation of optoelectronic and electronic devices [9–12]. In most of the nanostructure-based devices, the activation of such properties involves the application of an external voltage (V_{ext}), which in turn produces an EEF (E_{ext}). It is then crucial to deeply understand its impact on the internal electronic reconfiguration and the related modification on the QWRs and QDs properties.

Due to the issues related to the modeling of large (micrometric) wires and high electronic concentrations (around 10^{17} electrons/cm^3), most of the reported works address the study of an EEF on semiconductor nanostructures of small (nanometric) size, containing just one or a few electrons. So, when addressing QWRs, usually a transverse EEF is applied (along the short, nanometric, QWR cross-section) and single electronic or excitons redistribution, known as the Stark effect, are usually reported [13–19]. For example, for semiconductor QDs an electronic Stark shift (in the opposite direction to the EEF and towards lower energies), changes in the photoluminescense emission and optical absorption have been reported [17,18,20]. However, the most common configuration, when the EEF is applied along the wire remains much less studied mainly because it implies dealing with relatively large sizes and many-body electron-electron (*e*-*e*) interactions, which is a quite challenging issue.

In recent publications, we proposed the use of a Yukawa-like-interaction to deal with the many-body problem, which allows us to describe the *e*-*e* interaction in *n*-doped semiconductor nanostructures of typical electronic concentrations and realistic lengths [21,22]. By using this formalism, for example, valuable information about the Wigner molecule formation in QWRs, such as critical electronic-densities or optimal geometries were reported for different semiconductor materials. In the present work, we study the effect of an E_{ext} on the electronic distribution in semiconductor GaAs/AlGaAs nanostructures. To this end, the *e*-*e* is handled as in Ref. [22] while the E_{ext} is decoupled by applying it to the electronic center-of-mass framework of the entire *e*-*e* interacting system.

Hereafter, we solve the Schrödinger equation by decoupling the *e*-*e* relative framework from the center-of-mass one of the total electronic distribution. In the two-electron framework, two nonrelativistic electrons in GaAs wells

*reyna.mendez@uaslp.mx
†esteban.cruz@uaslp.mx

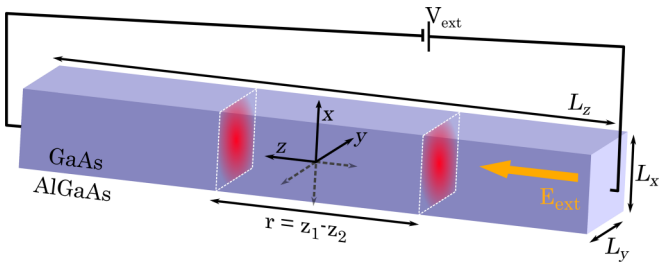

FIG. 1. Schematic illustration of the GaAs nanostructure of length L_z and cross section $L_x \cdot L_y$, embedded into a matrix of AlGaAs. All the plots in this paper are only for schematic purposes and not to scale.

embedded into an $Al_xGa_{1-x}As$ matrix are considered. The *e-e* interaction is described by a Yukawa-like potential, which captures the effect of many carriers through a screening parameter κ. By modifying κ, we can establish the carrier density n associated with the intentional n-doping level of epitaxially grown GaAs/AlGaAs nanostructures. The effect of a Coulombic V_{ext}, associated to the E_{ext}, which is applied on the center-of-mass framework of the *e-e* global interacting system is theoretically investigated.

II. THEORETICAL MODEL

A. Uncoupling the frameworks

We consider a square GaAs QWR embedded in a AlGaAs matrix (see Fig. 1). The time-independent Schrödinger equation for the two-electron wave function $\Psi(\vec{r}_1, \vec{r}_2) \equiv \Psi$ is given by [21,22]

$$-\frac{\hbar^2}{2m_e^*}\nabla^2\Psi + (V_{\text{eff}} + V_{\text{ext}})\Psi = E\Psi, \tag{1}$$

where $\hbar \equiv h/2\pi$, h is the Planck constant, m_e^* is the effective electron mass, and $V_{\text{eff}} = V_{e\text{-}w}(x, y) + V_{e\text{-}e}(r)$ is the electrostatic interaction potential. Here, $V_{e\text{-}w}$ (electron-wall) accounts for the transversal x and y finite square well potentials, and $V_{e\text{-}e}$ (electron-electron) is the longitudinal (along the z-axis) Yukawa-like interaction, which has the mathematical form

$$V_{e\text{-}e}(r) = \frac{e^2}{4\pi\epsilon\epsilon_0}\frac{\exp[-\kappa r]}{r}, \tag{2}$$

where $\epsilon = \epsilon_0\epsilon_r$, with ϵ_0 and ϵ_r being the vacuum permittivity and the dielectric constant of the material, respectively. Here r is the electron-electron separation distance (along the z-axis) and κ the screening parameter, given by [23]

$$\kappa = \sqrt{\frac{2e^2n}{\epsilon_0\epsilon k_B T}}, \tag{3}$$

with e the electron charge, n the electronic density, k_B the Boltzmann constant, and T the temperature. For simplicity, we consider the pair of electrons to be located along the z-axis. Thus, their relative distance is given by $r = z_1 - z_2$ and $V_{e\text{-}e}(r) = V_{e\text{-}e}(z)$.

The Coulombic V_{ext} in Eq. (1) is associated with the external potential along the z-axis, given by

$$V_{\text{ext}}(z) = eE_{\text{ext}}(z_1 + z_2), \tag{4}$$

TABLE I. Parameters of the GaAs and AlGaAs bulk materials, used in this work to solve Eqs. (12) and (13).

Parameter	GaAs	$Al_xGa_{1-x}As$
2Ry	10.78 meV	15.12 meV
a_B	10.26 nm	7.67 nm
m_e^*	0.0665 m_e	0.0857 m_e
$V_{e\text{-}w}$	0	186.42 meV
ϵ_r	12.9	12.247
T	300 K	
x	0	0.23

where E_{ext} is the external electric field. To solve Eq. (1), we consider the position of the center of mass $R = \frac{(z_1+z_2)}{2}$ and the reduced mass $\mu = \frac{m_e^*}{2}$. Then by using

$$z_1 = R + \frac{r}{2}, \tag{5}$$

$$z_2 = R - \frac{r}{2}, \tag{6}$$

one can redefine the operators and V_{ext} in terms of r and R as,

$$\nabla_1 = \nabla_r + \tfrac{1}{2}\nabla_R, \tag{7}$$

$$\nabla_2 = -\nabla_r + \tfrac{1}{2}\nabla_R, \tag{8}$$

$$V_{\text{ext}}(z) \equiv V_{\text{ext}}(R) = eE_{\text{ext}}2R. \tag{9}$$

Then, Eq. (1) can be rewritten as

$$\left[-\frac{\hbar^2}{4m_e^*}\nabla_R^2 + V_{\text{ext}}(R) - \frac{\hbar^2}{2\mu}\nabla_r^2 + V_{\text{eff}}(r)\right]\Psi = E\Psi. \tag{10}$$

By introducing $\Psi \equiv \Psi_{ij} = \chi_i(R)\gamma_j(r)$, Eq. (10) takes the form

$$\left[-\frac{\hbar^2}{4m_e^*}\nabla_R^2 + V_{\text{ext}}(R) + V_{e\text{-}w}\right]\chi_i(R)\gamma_j(r) + \left[-\frac{\hbar^2}{2\mu}\nabla_r^2 + V_{e\text{-}e}(r)\right]\chi_i(R)\gamma_j(r) = E\,\chi_i(R)\gamma_j(r), \tag{11}$$

where the energy $E = E_R + E_r$ contains the contributions from both frameworks. Eqquation (11) can be reduced to the two independent and simpler equations

$$\left[-\frac{\hbar^2}{4m_e^*}\nabla_R^2 + V_{\text{ext}}(R) + V_{e\text{-}w}\right]\chi_i(R) = E_R\chi_i(R), \tag{12}$$

and

$$\left[-\frac{\hbar^2}{2\mu}\nabla_r^2 + V_{e\text{-}e}(r)\right]\gamma_j(r) = E_r\gamma_j(r). \tag{13}$$

Here, Eq. (12) contains the EEF contribution in the center-of-mass framework and Eq. (13) the *e-e* and *e-w* contributions in the two-electron relative framework. In Table I the parameters used to solve these equations are summarized.

B. Center-of-mass framework solution

Equation (12) is solved by considering infinite barriers at the edges of the structure (on the z-axis, where $V_{e\text{-}w} = 0$), and the E_{ext} is applied along the z-axis on a particle of mass $2m_e^*$.

For such conditions, the solution is analytical, and has the form

$$\chi_i(R) = Ai\left(\frac{(2eRE_{\text{ext}} - E_{R_i})m_e^*}{\hbar^2\left(\frac{eE_{\text{ext}}m_e^*}{\hbar^2}\right)^{2/3}}\right)C_{1i} + Bi\left(\frac{(2eRE_{\text{ext}} - E_{R_i})m_e^*}{\hbar^2\left(\frac{eE_{\text{ext}}m_e^*}{\hbar^2}\right)^{2/3}}\right)C_{2i}, \tag{14}$$

where Ai, Bi are the Airy functions, C_{1i} and C_{2i} are normalization constants, and the index $i = 1, 2, 3, \ldots$ defines the quantum state. In this paper, we only analyze the ground ($i = 1$) and first excited state ($i = 2$).

By considering the infinite barrier boundary condition $\chi_i(\pm\frac{L_z}{2}) = 0$ and defining $\alpha = \frac{m_e^*}{\hbar^2}\left(\frac{eE_{\text{ext}}m_e^*}{\hbar^2}\right)^{-2/3}$, we get

$$Ai([eE_{\text{ext}}L_z - E_{R_i}]\alpha)C_{1i} + Bi\big([eE_{\text{ext}}L_z - E_{R_i}]\alpha\big)C_{2i} = 0, \tag{15}$$

and

$$Ai([-eE_{\text{ext}}L_z - E_{R_i}]\alpha)C_{1i} + Bi\big([-eE_{\text{ext}}L_z - E_{R_i}]\alpha\big)C_{2i} = 0, \tag{16}$$

which can be used to determine the eigenenergies as a transcendental equation. The ratio C_{1i}/C_{2i} can be calculated from

$$\frac{Bi\big([eE_{\text{ext}}L_z - E_{R_i}]\alpha\big)}{Ai\big([eE_{\text{ext}}L_z - E_{R_i}]\alpha\big)} = \frac{Bi\big([-eE_{\text{ext}}L_z - E_{R_i}]\alpha\big)}{Ai\big([-eE_{\text{ext}}L_z - E_{R_i}]\alpha\big)}. \tag{17}$$

C. Electron-electron framework solution

By considering infinite barriers at the nanostructure's z-edges, an error in the calculation is introduced, which is particularly important for QDs. Focusing on usual n-GaAs/metal Schottky barriers, we estimated typical errors around 4–10% for the smaller nanostructures studied in this contribution. This error does not modify the main conclusions of this work.

The solution of Eq. (13), corresponding to the two-electron framework $[\gamma_j(r),\ j = 1, 2, 3, \ldots]$, can be numerically obtained by using the finite differences method (e.g., see Ref. [21]). Due to the strongly confined condition in the x-y plane (L_x and L_y are set to 8 nm), we only consider the ground state. The solutions are well known [24]:

$$\psi(w) = \begin{cases} N_w \cos(w l_w) & w \leqslant |L_w/2|, \\ C_w e^{w m_w} + D_w e^{-w m_w} & w \geqslant |L_w/2|, \end{cases} \tag{18}$$

where $w = x$ or y; N_w, C_w, D_w are normalization constants, $l_w = \sqrt{\frac{2\mu E_w}{\hbar^2}}$, $m_w = \sqrt{\frac{2\mu(V_{e\text{-}w} - E_w)}{\hbar^2}}$, and E_w the eigenenergy.

III. EEF ELECTRONIC REDISTRIBUTION

We expect that an E_{ext} acting on a negative distribution of charge should shift it to the opposite direction to the EEF. As we discuss further below, this is observed for the ground and excited states (together with the deformation of the original symmetrical charge distribution due to the interaction with the edge of the wire) when we only consider the center-of-mass framework. However, when the e-e and e-w components are added to the EEF, the behavior becomes more complex for the excited states' distributions.

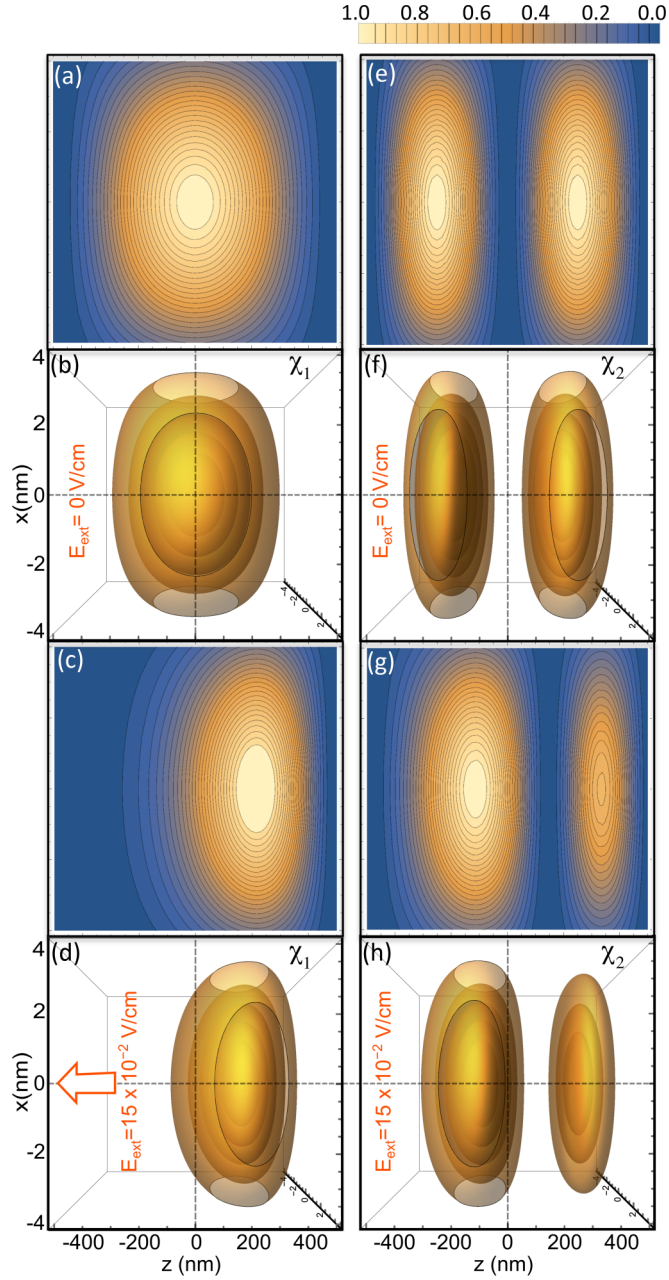

FIG. 2. 3D plots and 2D contour plots displaying the electronic distribution inside a GaAs/AlGaAs QWR of dimensions $L_{x,y} = 8$ nm and $L_z = 1\,\mu$m. In the upper rows the distributions correspond to the [(a) and (b)] ground (χ_1) and [(e) and (f)] first excited (χ_2) states without an external force. The lower rows [(c), (d), (g) and (h)] shows the effect of the EEF (of magnitude $E_{\text{ext}} = 1.5 \times 10^{-1}$ V/cm), which is applied along the $-z$ direction on the electronic center-of-mass.

In Fig. 2, three-dimensional (3D) plots and two-dimensional (2D) contour plots corresponding to the probability densities for the ground (χ_1) and first excited states (χ_2), as calculated from Eq. (12) are presented. In the lower row, it can be observed the shift of the charge distribution produced by an E_{ext} of magnitude 1.5×10^{-1} V/cm. The plots in Fig. 2 correspond to a QWR of $L_{x,y} = 8$ nm and $L_z = 1\,\mu$m. For

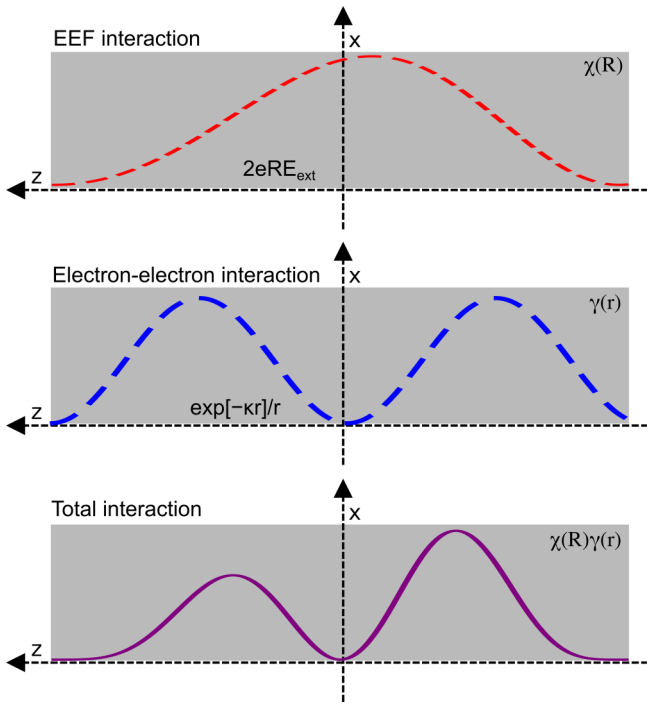

FIG. 3. Schematic representation of the two different frameworks used to model the total interaction inside the semiconductor nanostructures, that is, the external electric field plus the *e-e* and *e-w* interactions.

QDs (L_z around 10–20 nm) a similar trend is observed, but higher E_{ext} values are needed (E_{ext} around 10^3 V/cm).

Without the influence of an EEF, symmetrical and truncated electronic distributions are observed in the center-of-mass framework, as expected. The truncated features in the 3D projections results from tunneling, discernible for small-enough cross-section values ($L_{x,y} < 30$ nm), as finite barriers at the GaAs/AlGaAs ($x - y$) interfaces were considered. The symmetrical distributions are lost as the electrons redistribute by the influence of EEF and by the interaction with the infinite barriers at the z-edges [see Figs. 2(c) and 2(d) and 2(g) and 2(h)].

IV. COUPLING THE FRAMEWORKS

What is of interest in this work is to describe the total influence on the electronic density due to the external electric field the *e-e* interaction and the quantization effects due to the nanometric size of the GaAs/AlGaAs structures. The EEF influence on the total electronic distribution [related to $|\chi_i(z)|^2$] was described in the previous section. In Ref. [22], the *e-e* Coulombic interaction and the quantum confinement [related to $|\gamma_j(z)|^2$] were extensively examined by using an effective potential, which includes the Yukawa-like interaction and the x-y confinement. In this section, we will describe the electronic distribution by coupling both frameworks [related to $|\chi_i(z)|^2|\gamma_j(z)|^2$], which is schematically illustrated in Fig. 3.

We first consider a QWR of length $L_z = 1\,\mu$m, cross-section $L_{x,y} = 8$ nm, and $n_1 = 10^{17}$ cm^{-3}. To facilitate the discussion, we consider two different EEF magnitude intervals. One for weak EEFs (from 0 to 150 mV/cm, where the charge redistributes without considerable influence of the barrier at the z-edge, see Fig. 4) and the other for strong EFF

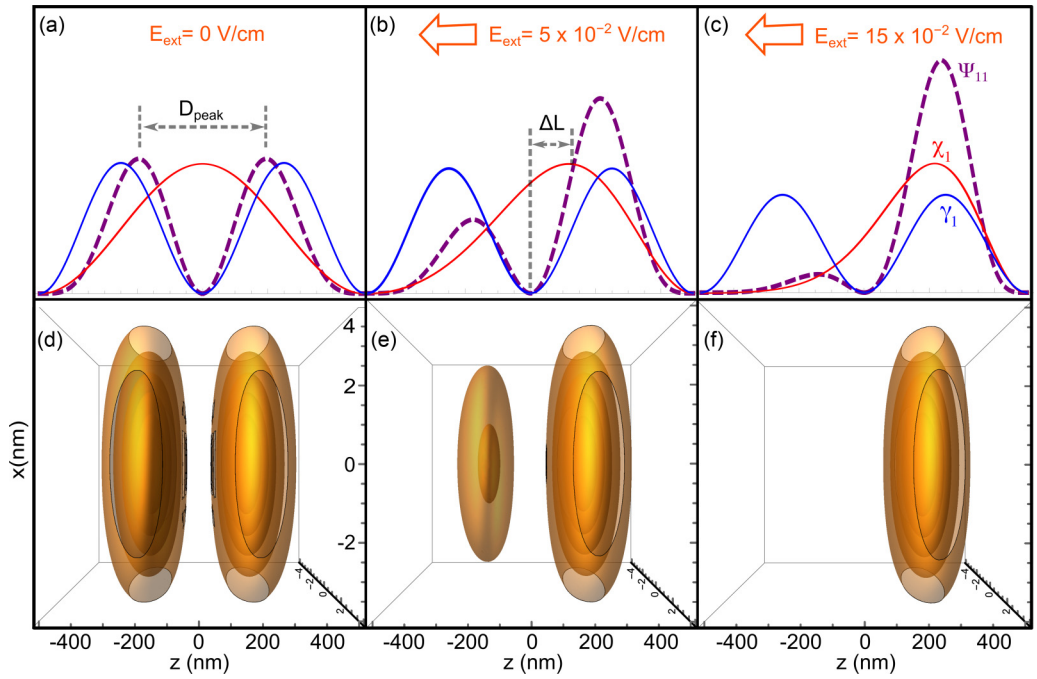

FIG. 4. Electronic distribution for the ground state (Ψ_{11}) of a GaAs/AlGaAs QWR of size $L_{x,y} = 8$ nm and $L_z = 1\,\mu$m, which contains both the external E_{ext} (χ_1) and the *e-e* and *e-w* interactions (γ_1). For clarity, in the upper row, the profiles corresponding to each component and the total distributions are displayed. The electronic concentration was set to 10^{17} cm^{-3} and the E_{ext} was applied pointing to the $-z$ direction.

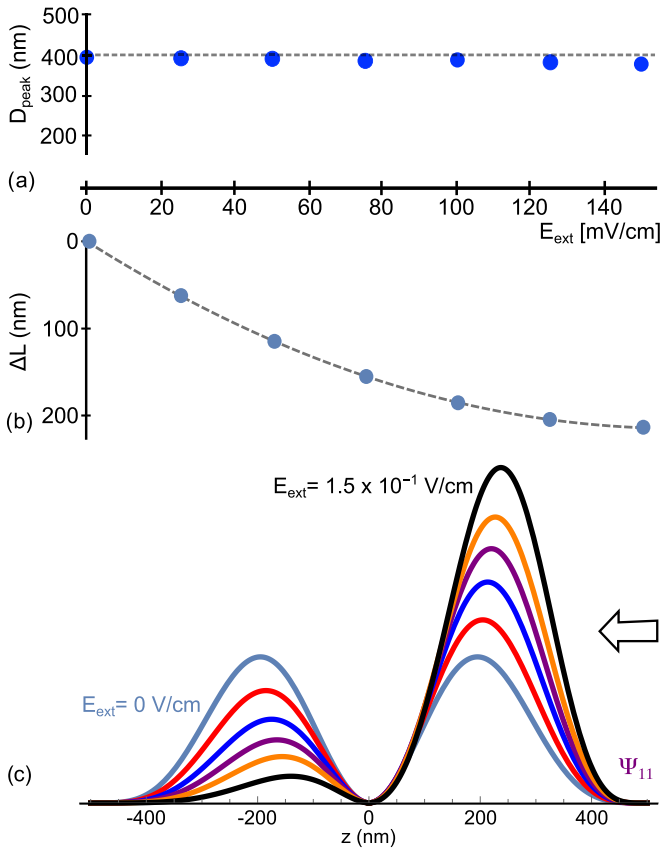

FIG. 5. (a) D_{peak}, (b) ΔL dependence of the charge distribution, and (c) the probability density, for the ground state in a QWR for different values of E_{ext} (< 150 mV/cm, weak regimen). Here $L_{x,y} = 8$ nm, $L_z = 1\,\mu$m, and n $= 10^{17}$ cm^{-3}.

values (above 300 mV/cm, where the z-barrier affects the redistribution, see Fig. 6).

A similar weak/strong analysis can be done for others nanostructure settings (but different values for the weak and strong EEFs must be considered). For example, for $L_z = 30$ nm, $L_{x,y} = 8$ nm and $n_1 = 10^{17}$ cm^{-3} a strong EEF must have a value larger than 5 kV/m (because of the strong quantum confinement on the z-axis).

A. General behavior

In Fig. 4, the electronic probability density for the ground state ($|\Psi_{11}|^2$) for weak EEFs is displayed. For clarity, we plot in the upper row [Figs. 4(a) to 4(c)] the profile of each component of the distributions presented in the lower row [Figs. 4(d) to 4(f)]: the EEF acting on the center-of-mass framework [$|\chi_1(z)|^2$, blue solid line], the e-e interaction and x-y confinement in the e-e framework [$|\gamma_1(z)|^2$, red solid line], and the coupled frameworks [$|\Psi_{11}|^2 = |\chi_1(z)|^2|\gamma_1(z)|^2$, purple dashed line].

As can be observed in Fig. 4, the coupled system incorporates the electronic shift due to the EEF in a clear way. The e-e interaction and the x-y confinement, which trigger the formation of a two-peak profile (see Ref. [22]) is correctly contained in the global $|\Psi_{11}|^2$.

D_{peak}, i.e., the distance between the two-peaks in $|\Psi_{11}|^2$ [see Fig. 4(a)], is a parameter that describes the relative shift induced by the EEF. In Fig. 5(a) this parameter is plotted for different values of E_{ext} in the weak regimen. As observed, in the absence of an EEF $D_{\text{peak}} \sim 400$ nm and it slowly and linearly decreases as the magnitude of E_{ext} increases. Then, basically the EEF transfers the charge from one of the two peaks to the other (in this case, to the $+z$ region), preserving almost without changing the distance between the two peaks.

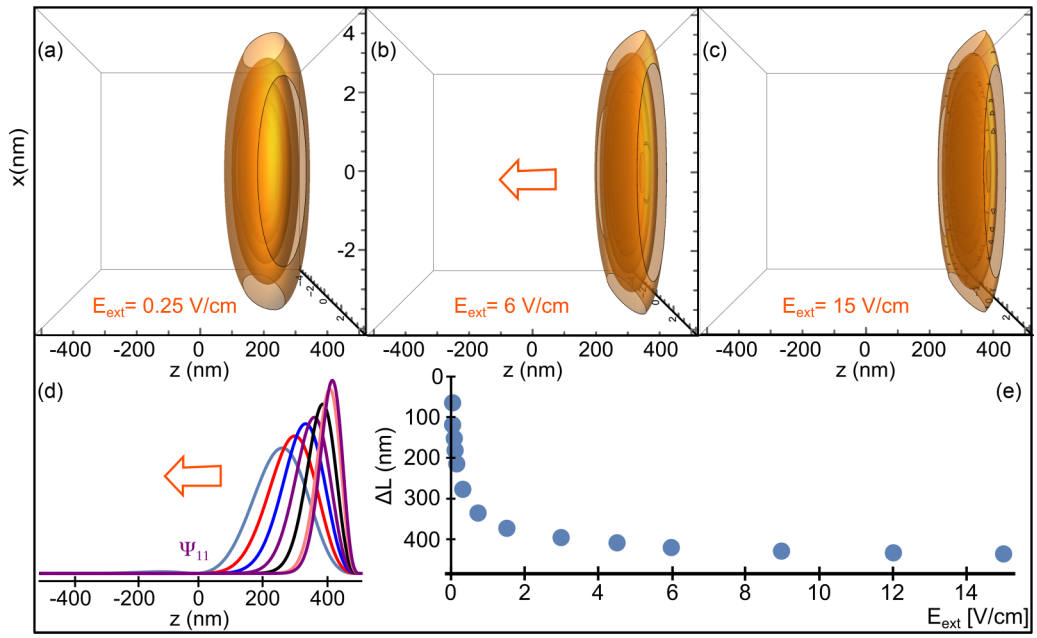

FIG. 6. (a)-(c) 3D electronic density plots, (d) 2D profiles, and (e) ΔL dependence corresponding to the ground state of a QWR under different values of E_{ext} (>150 mV/cm, strong regimen). The dimensions of the QWR are $L_{x,y} = 8$ nm, $L_z = 1\,\mu$m, and doping level $n = 10^{17}$ cm^{-3}.

In contrast, if the shift of the electronic center-of-mass ΔL [see Fig. 4(b)] is considered, a notable displacement is found, as displayed in Fig. 5(b). In Fig. 5(c), the continuous modification of $|\Psi_{11}|^2$ when E_{ext} varies from 0 to 150 mV/cm is presented.

For larger EEF values ($E_{\text{ext}} > 150$ mV/cm) a different behavior is observed (see Fig. 6). As the charge is concentrated in only one peak, on the $+z$ region of the QWR, the main effect of the EEF is to squeeze the electronic distribution towards the $+z$ QWR edge. Figure 6(d) shows the changes in the probability density for the coupled system as a function of E_{ext} within the strong coupling regimen. As observed in Figs. 6(a) to 6(c), for stronger E_{ext} a disk-like charge distribution is induced. In such a case, the ΔL asymptotically shifts to a limited value (for the parameters used in the present configuration ΔL tends to ∼440 nm).

B. *n*-doping level dependence

In the previous sections, a value for κ corresponding to an n-doping level of 10^{17} cm^{-3} was considered, which is a GaAs doping level value usually used in devices and experimental setups. It is also the lower electronic density that our model can manage in a safe way (see Ref. [22]).

However, as higher doping concentrations can be easily obtained in real semiconductor nanostructures (for further applications), in this section we now explore the modification of the electronic distribution by an EEF in a QD ($L_z = 30$ nm) and a QWR ($L_z = 1\,\mu$m) with n-doping levels up to 10^{23} cm^{-3}. In each case, an E_{ext} in the weak range is used, as it provides more information than the stronger one. We consider both the ground and excited states Ψ_{12}, Ψ_{21}, and Ψ_{22}.

In Fig. 7 the profiles corresponding to Ψ_{11} for a QD and a QWR, for different values of E_{ext} and as a function of the n-doping level and their corresponding screening length $\lambda = 1/\kappa$, are shown. As can be observed, the dependence is more substantial for the QD, where a strong screening is observed even for the lower concentration. The well-defined independent two-peak distribution is a characteristic of QWR, related to the formation of the Wigner molecule. As observed, the molecule is destroyed by the EEF. We also observe that largest values of E_{ext} are needed for a QD to observe significant changes in the electronic distribution, which is related to the strong confinement of the carriers in the z-direction.

A simple way to quantify the effect of the E_{ext} on the redistribution of the charge is by calculating the amount of charge transferred from one side to the other (marked as {I} and {II} in Fig. 7) by the EEF. The electronic portion carried from the {II}region to the {I}region depends on the n-doping level and E_{ext}, but it is evident in the QD for the values chosen for E_{ext}, as displayed in Fig. 7, where the percentage of the original charge that is transferred is displayed for various values (without a EEF, the distribution is 50%–50%).

To visualize the different effects of the EEF on the excited states, in Fig. 8 the 2D contour plots of the probability density for the ground and the Ψ_{12}, Ψ_{21}, and Ψ_{22} excited states are displayed for a QWR ($L_z = 1\,\mu$m, $L_{x,y} = 8$ nm, and n $= 10^{17}$ cm^{-3}). The left column in Fig. 8 corresponds to $E_{\text{ext}} = 0$ and the right column to the case when a moderated $E_{\text{ext}} = 1.5 \times 10^{-1}$ V/cm is applied. As can be observed, now

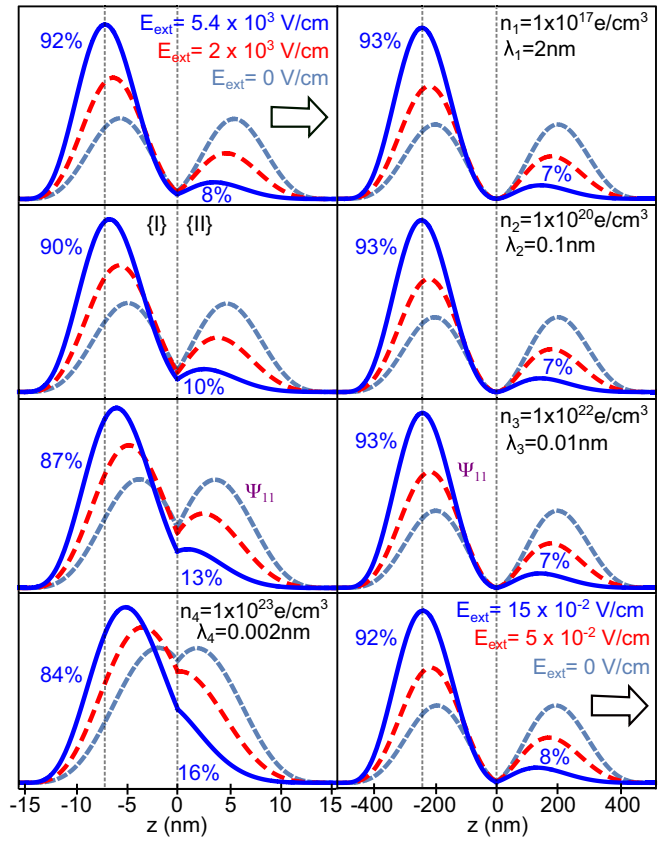

FIG. 7. Dependence of the ground-state electronic distribution with the n-doping level and a moderated E_{ext}. The 2D profiles of the left column correspond to a QD of dimensions $L_{x,z} = 8$ nm and $L_z = 30$ nm. The right column correspond to a QWR of dimensions $L_{x,z} = 8$ nm and $L_z = 1\,\mu$m. In both cases, for the stronger value of E_{ext} (in the blue-continuous line) the percentage of charge in each of the two-fold distribution is displayed. Vertical dotted lines help to visualize the shift of the distribution.

the behavior is not as simple as the one seen in the ground state.

As observed from Fig. 8, the electronic distributions display a symmetrical distribution with respect to the center of the QWR when $E_{\text{ext}} = 0$. However, when the EEF is applied, the charge redistribution does not exhibit a simple relocation at the QWR edge, which, as before, is only observed for the ground state and just partially for Ψ_{12}. For Ψ_{12}, the charge tends to be relocated at the $+z$ edge of the wire, nevertheless, most of the charge is localized at the third electronic distribution, not at the fourth, closer to the edge.

For Ψ_{21}, the charge redistributes in the opposite side of the wire. That is, the electronic charge moves in the opposite direction as one could expect. Furthermore, for Ψ_{21} an additional electronic distribution arises between the original two-fold distribution when the EEF is applied. For Ψ_{22} the redistribution of the charge is even more complex but similar to Ψ_{21}, as a new distribution appears and the charge tends to redistribute at the $-z$ side of the QWR.

Finally, one can also explore the effect that the electronic density has on the excited states. In Fig. 9, the Ψ_{12} excited state of a QD and a QWR is presented for various n-doping

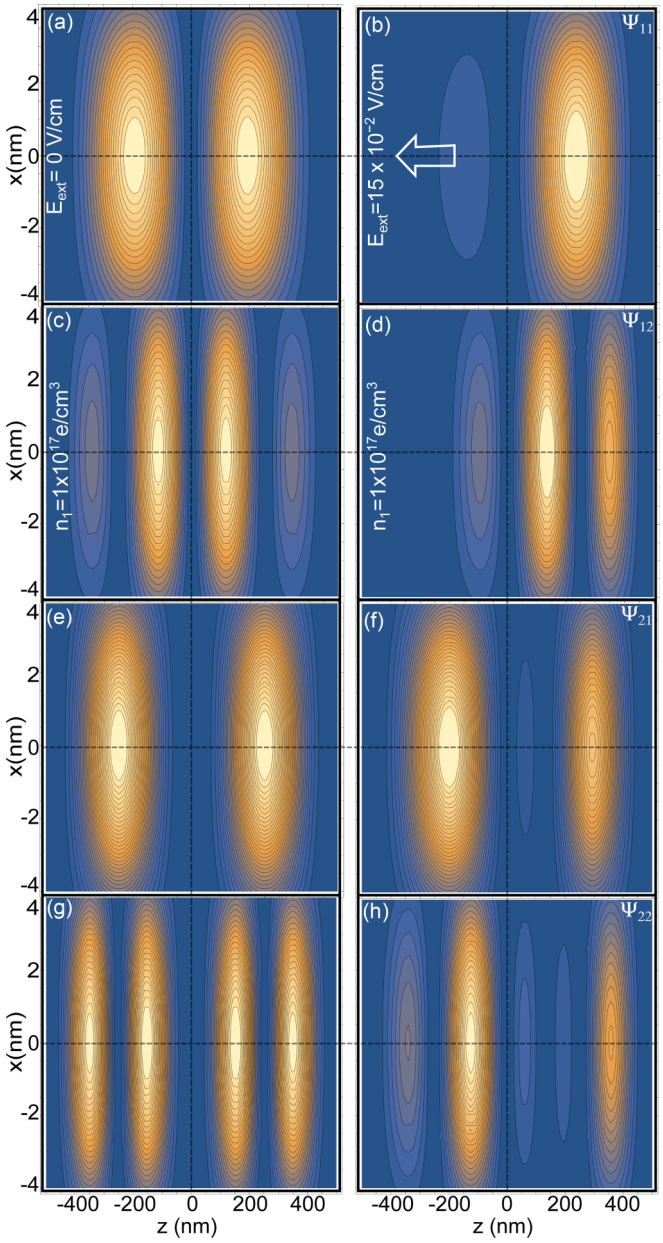

FIG. 8. 2D contour plot showing the charge distribution in a QWR for the ground (Ψ_{11}) and the three first excited (Ψ_{12}, Ψ_{21}, and Ψ_{22}) states. The left column displays the distributions without an EEF. The right column shows the effect of the application of an $E_{\text{ext}} = 15 \times 10^{-2}$ V/cm, which is set along the $-z$ direction.

concentrations and E_{ext} magnitudes (similar to Fig. 7, but for an excited state).

Aside from the obviously larger number of nodes in the electronic distribution, the general trend is quite similar to the observed for Ψ_{11} in Fig. 7: the n-doping level does not affect the QWR as it affects the QD and the charge redistributes by passing from one individual distribution to the next (to $-z$ in this case, with E_{ext} pointing to $+z$). Given the behavior of Ψ_{21} and Ψ_{22} in Fig. 8, one could expect a more complex behavior for higher excited states with the modification of the n-doping level.

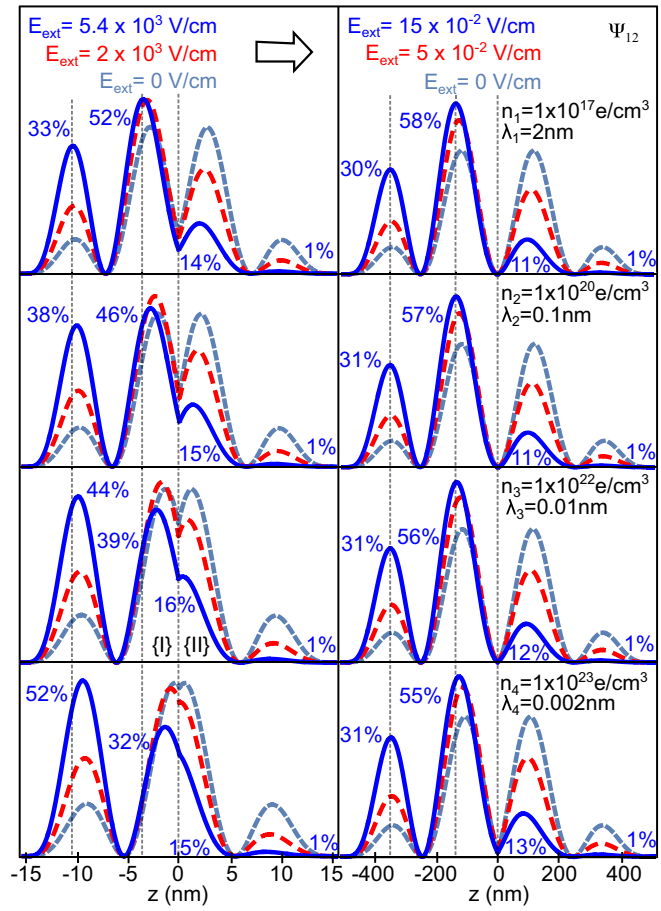

FIG. 9. Dependence of the Ψ_{12} excited state distribution with the n-doping level and a moderated E_{ext}. The 2D profiles of the left column correspond to a QD of dimensions $L_{x,z} = 8$ nm and $L_z = 30$ nm. The right column corresponds to a QWR of size $L_{x,z} = 8$ nm and $L_z = 1\,\mu$m. In both cases, for the stronger value of E_{ext} (in the blue-continuous line) the percentage of charge in each of the four-fold distributions is displayed.

V. CONCLUSION

In summary, we theoretically investigated the effect of an EEF on the ground and excited states of a system of many electrons confined in GaAs nanostructures. Our theoretical approximation allows us to observe the effect of the EEF in a easy way in nanostructures of various sizes and electronic concentrations. This alternative approach also allows us to decouple the e-e and the EEF interactions, which results as being useful in determining the origin of the observed features. We showed that this approach is well suited to get relevant information in semiconductor nanostructures of realistic sizes and practical doped levels. Interesting and unexpected redistributions by the EEF are observed for some excited states. Experimental studies are in process to verify our predictions.

ACKNOWLEDGMENTS

The authors acknowledge financial support from Consejo Nacional de Ciencia y Tecnología (CONACyT; Grants No. FC2016-01/2408, No. CB2015-01/1257434,

No. CB2014/237425, and No. CB2016-01/287067) and PRODEP (Grant No. 511-6/17-4023). R.C.-P. also acknowledges the financial support provided by the Marcos Moshinsky Foundation.

[1] Z. Dong, Y. André, V. G. Dubrowskii, C. Bougerol, C. Leroux, M. R. Ramdani, G. Monier, A. Trassoudaine, D. Castelluci, and E. Gil, Nanotechnology **28**, 125602 (2017).
[2] J. N. Tiwari, R. N. Tiwari, and K. S. Kim, Prog. Mater. Sci. **57**, 724 (2012).
[3] Y. Xia, P. Yang, Y. Sun, Y. Wu, B. Mayers, B. Gates, Y. Yin, F. Kim, and H. Yan, Adv. Mater. **15**, 353 (2003).
[4] A. Mostofizadeh, Y. Li, B. Song, and Y. Huang, Journal of Nanomaterials **2011** 685081 (2011).
[5] A. A. Zhukov, C. Volk, A. Winden, H. Hardtdegen, and T. Schäpers, JETP Lett. **100**, 32 (2014).
[6] V. D. Vikram and B. Marc, Nat. Phys. **4**, 314 (2008).
[7] N. T. Ziani, F. Cavaliere, and M. Sassetti, New J. Phys. **15**, 063002 (2013).
[8] S. A. Soffing, M. Bortz, I. Schneider, A. Struck, M. Fleischhauer, and S. Eggert, Phys. Rev. B **79**, 195114 (2009).
[9] X. L. Wang and V. Voliotis, J. Appl. Phys. **99**, 121301 (2006).
[10] Y. Arakawa and H. Sakaki, Appl. Phys. Lett. **40**, 939 (1982).
[11] H. Sakaki, Jpn. J. Appl. Phys. **19**, L735 (1980).
[12] R. R. LaPierre, A. C. E. Chia, S. J. Gibson, C. M. Haapamaki, J. Boulanger, R. Yee, P. Kuyanov, J. Zhang, N. Tajik, N. Jewell, and K. M. A. Rahman, Phys. Status Solidi RRL **7**, 815 (2013).
[13] C. X. Xia and H. N. Spector, J. Appl. Phys. **105**, 084313 (2009).
[14] T. Y. Zhang and W. Zhao, Phys. Rev. B **73**, 245337 (2006).
[15] J. Lee, H. N. Spector, W. C. Chou, and Y. S. Huang, Phys. Rev. B **72**, 125329 (2005).
[16] G. H. Wang, Phys. Rev. B **72**, 155329 (2005).
[17] T. Arakawa, Y. Kato, F. Sogawa, and Y. Arakawa, Appl. Phys. Lett. **70**, 646 (1997).
[18] H. N. Spector and J. Lee, Physica B **393**, 94 (2007).
[19] E. P. Pokatilov, V. A. Fonoberov, S. N. Balaban, and V. M. Fomin, J. Phys.: Condens. Matter **12**, 9037 (2000).
[20] W. Sheng, K. Yun, and H. Chunjie, J. Semicond. **34**, 102001 (2013).
[21] R. Méndez-Camacho, E. Cruz-Hernández, and R. Castañeda-Priego, Phys. Rev. B. **95**, 085437 (2017).
[22] R. Méndez-Camacho, E. Cruz-Hernández, and R. Castañeda-Priego, Phys. Rev. B. **100**, 085438 (2019).
[23] E. Stern, R. Wagner, F. J. Sogworth, R. Breaker, T. M. Fahmy, and M. A. Reed, Nano Lett. **7**, 3405 (2007).
[24] H. Paul, *Quantum Wells, Wires and Dots: Theoretical and Computational Physics of Semiconductor Nanostructures*, 2nd ed. (Wiley, West Sussex, England, 2006).